

# The Dynamics of Vortices on Gas Giants - A Case Study with Jupiter

Tanisha Ghosal and Hayley Kavanagh

April 13, 2023

## Abstract

This report presents an approach to two-dimensionally simulate the vortices on gas giant planets, with a particular focus on Jupiter. Jupiter's atmosphere is well-known for its complex and dynamic patterns of vortices, and understanding the behaviour of these structures is crucial for understanding the planet's weather patterns and atmospheric dynamics. Using a 1-layer shallow water model with the pseudospectral (Fourier) method and Adams-Bashforth time-stepping, we demonstrate the ways in which vortices evolve over time and interact with one another in Jupiter's atmosphere. In particular, we investigate the vortex interactions for three cases of the initial number of vortices: two vortices, three vortices, and six vortices. Our results shed light on the dynamics of dipole and tripole vortices, and how they may emerge from the hexagonal patterns seen on Jupiter's atmosphere, and additionally offer insights into the behaviour of vortices in other gas giant atmospheres.

## 1 Introduction

Vortex dynamics on gas giants such as Jupiter are characterized by the swirling movement of gases in their atmospheres. These movements can lead to the formation of stable and cohesive structures called vortices, which can greatly influence the weather patterns and atmospheric dynamics of these planets.

The formation of vortices on gas giants is thought to be driven by a combination of factors, including the rotation of the planet, the variation in temperature and pressure across the atmosphere, and the presence of instabilities that can trigger the formation of vortices. The dynamics of vortices on gas giants are complex and can involve a range of processes, including advection, diffusion, and turbulent mixing. These processes can impact the transport of heat and energy in the atmosphere, the distribution of atmospheric gases, and the weather patterns on these planets.

In this investigation, we aim to produce a vorticity map for the scenarios of a single vortex with different shapes, and the interaction between two vortices. This map will be produced from a Python code that uses a two-dimensional, one-layer shallow water model.

## 2 Theoretical Background

One important instability that thought to be responsible for the formation of vortices is the baroclinic instability, which arises due to the variation of temperature and pressure with height in the atmosphere. This instability can lead to the formation of vortices at different scales, from small eddies to large-scale vortices like the Great Red Spot. The mathematical derivation of this instability and the conditions for its occurrence are explored further.

### 2.1 Elemental Equations and Properties

We can enforce the conservation of a few different properties for the environment, some of which include energy, momentum and angular momentum. The conservation of energy in its most general form can be expressed as,

$$\frac{\partial \rho e}{\partial t} + \nabla \cdot [\rho \mathbf{v}(e + \frac{p}{\rho}) + \mathbf{F}_q - \mathbf{v}\boldsymbol{\sigma}] = \rho q \quad (1)$$

These equations given below govern the hydrostatic vertical momentum and are enforced by the property of conservation of momentum.

$$\rho \frac{D\mathbf{v}}{Dt} + 2\boldsymbol{\Omega} \times \mathbf{v} = -\frac{1}{\rho} \nabla p - \nabla \Phi + \frac{1}{\rho} \nabla \cdot \boldsymbol{\Omega} \quad (2)$$

The angular momentum, or the axial component of the momumentum, of any fluid particle will be guided by the balance of the following equation,

$$\frac{\partial \rho m}{\partial t} + \nabla \cdot (\rho m \mathbf{v}) = \frac{\partial m}{\partial t} + \mathbf{v} \cdot \nabla m \quad (3)$$

Initially, if we take constant density, viscosity and incompressible flow, we obtain the continuity equation:

$$\frac{\partial \rho}{\partial t} + \nabla \cdot (\rho \mathbf{u}) = 0 \quad (4)$$

## 2.2 Vortex Dynamics

In this section, we will discuss the fundamental equations that govern the physical processes in fluid motion and circulation. These equations focus on the main properties of vortices, such as the circulation and vorticity.

### 2.2.1 Vorticity

Vorticity is a fundamental concept in fluid mechanics that describes the local rotation of fluid elements in a flow. In its simplest form, vorticity is the curl of the velocity vector of a fluid particle. Taking the curl of the Navier Stokes Equation generates the following vorticity equations:

For ideal flow,

$$\frac{\partial \omega}{\partial t} = \nabla \times (\mathbf{u} \times \omega) \quad (5)$$

$$\frac{D\omega}{\partial t} = \omega \cdot \nabla \mathbf{u} \quad (6)$$

- $\Omega$  is the value of the Coriolis force
- $\gamma$  is the gradient of the Coriolis parameter

For non-zero viscosity,

$$\frac{D\omega}{\partial t} = \omega \cdot \nabla \mathbf{u} + \nu \nabla^2 \omega \quad (7)$$

### 2.2.2 Vortex Filament, Tube and Flux

In fluid mechanics, a vortex filament, or vortex line, 2.2.2 is a mathematical construct used to represent a thin, infinitely long, and perfectly smooth line of vorticity in a fluid flow. The vorticity in the filament induces a velocity field around the filament, which in turn generates a circulation around the filament. The circulation is defined as the line integral of the fluid velocity around the filament.

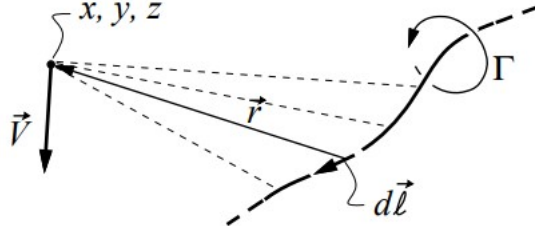


Figure 1: Vortex Line illustration.

Mathematically, the vorticity in the filament can be represented by the Biot-Savart law, which relates the velocity induced by the vorticity at a point in space to the vorticity at another point in space. In the case of a vortex filament, the Biot-Savart law can be written as:

$$\frac{d\mathbf{x}}{ds} = |\boldsymbol{\omega}|[\mathbf{x}(s)] \quad (8)$$

where  $v(r)$  is the velocity induced at a point  $r$  in space,  $\Gamma$  is the circulation around the filament,  $r_0$  is a point on the filament, and  $x$  denotes the vector cross product. The velocity induced by the filament at a point  $r$  in space is perpendicular to the vector  $(r - r_0)$  and has a magnitude proportional to  $\frac{\Gamma}{|r - r_0|}$ .

For a vortex tube, shown in Figure 2.2.2, the curl lacks divergence and therefore follows that,

$$\nabla \cdot \boldsymbol{\omega}_a = 0 \quad (9)$$

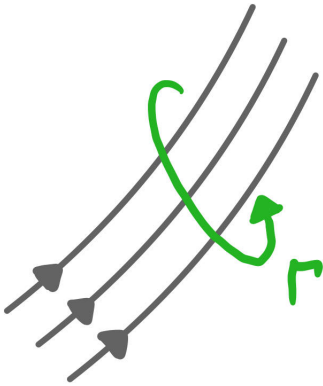


Figure 2: The line vortex in two dimensions can be integrated over its length such that the arc length element  $d\ell$  is flows parallel to the filament, for the direction of positive circulation (Archatz, Figure 2.1).

Physically, vortex filaments are lines that represent the centerlines or axes of the vortices, while vortex tubes are the three-dimensional structures that enclose the vortices. These are often used to describe a phenomenon known as vortex shedding. Vortex shedding refers to the periodic shedding of vortices from a bluff body as it moves through a fluid, creating an alternating pattern of vortices in the wake of the body. These vortices are typically formed as the fluid flows around the body and separates from its surface, leading to the formation of organized structures in the wake. In the context of vortex shedding, the vortices that are shed from the bluff body can be visualized as vortex filaments that are periodically shed from the surface of the body and transported downstream in the wake. These vortex filaments can sometimes merge and form vortex tubes, which are elongated structures that enclose the vortices and define their boundaries.

### 2.2.3 Biot-Savart

In the context of fluid mechanics, the Biot-Savart law describes the vorticity generated by a small element of fluid and how it contributes to the vorticity of the overall flow. It is given by:

$$\boldsymbol{\omega} = \frac{1}{4\pi} \frac{\delta \mathbf{v} \times \mathbf{r}}{r^3} dV \quad (10)$$

The Biot-Savart equation is a powerful tool for understanding the vorticity dynamics of fluid flows. It can be used to analyze the vorticity produced by different sources, such as turbulence, and to study the interaction between vortices in a flow. Additionally, the Biot-Savart equation can be combined with the Navier-Stokes equations to provide a complete description of the flow field.

#### 2.2.4 Helmholtz' Theorem

The Helmholtz theorem is a fundamental concept in vector calculus that describes the decomposition of a vector field into a curl-free component and a divergence-free component. In fluid mechanics, this theorem is particularly important because it relates the velocity field to the vorticity field.

The Helmholtz theorem states that any sufficiently smooth, continuous, and bounded vector field can be decomposed into a curl-free component and a divergence-free component. In fluid mechanics, the Helmholtz theorem relates the velocity field to the vorticity field through the use of the vector potential. By taking the curl of the Navier-Stokes equation, one can derive a differential equation for the vorticity field in terms of the velocity field and its derivatives. By applying the Helmholtz decomposition to the velocity field, the vorticity field can be expressed in terms of the curl of the vector potential:

$$\omega = \nabla \times v = \nabla \times (\nabla \times A) = \nabla(\nabla \cdot A) - \nabla^2 A \quad (11)$$

where  $\omega$  is the vorticity field.

#### 2.2.5 Circulation

We can characterize fluids based on their local properties, one of them being vorticity, which suggests the magnitude of a fluid's rotation. Associated with this vorticity property is the circulation, which can be expressed by the following closed line integral along some curve  $C$ ,

$$\Gamma = \oint_C \mathbf{v}(\mathbf{x}, t) \cdot d\ell \quad (12)$$

- Such that the absolute flux describes the strength of the vortex (tube),

$$flux = \int_{dS} \mathbf{n} \cdot \omega \quad (13)$$

Thus, for a closed path around a vortex, we can assume circulation to be the line integral of a fluid particle's velocity. The material derivative of this circulation function can be decomposed into two main components, the Coriolis force and the Kelvin Circulation, as shown below:

$$\frac{D\Gamma}{Dt} = - \oint_C (2\boldsymbol{\omega} \times \mathbf{v}) \cdot d\mathbf{x} - \oint_C \frac{1}{\rho} \nabla p \cdot d\mathbf{x} + \oint_C \frac{1}{\rho} (\nabla p \cdot \boldsymbol{\sigma}) \cdot d\mathbf{x} \quad (14)$$

- Where the first component on the right hand side of the equation goes to zero for non-baroclinic, or barotropic flow ( $\nabla\rho = \frac{1}{\rho}\nabla p$ ), and thus describes the baroclinicity of the system.
- The Coriolis Force, suggested by the two most right terms, is generated by the Coriolis parameter,

$$fV = -\frac{\partial \Phi}{\partial n} \quad (15)$$

We can introduce Kelvin's theorem regarding the circulation of fluids. This theorem suggests that for fluids with negligible viscous shear and normal-stresses (inviscid fluids), we can take the circulation to be independent of time, for all closed material curves. This simply requires that for a fluid with ideal flow,

$$\frac{D\Gamma}{Dt} \equiv \frac{d\Gamma(C(t), t)}{dt} = 0 \quad (16)$$

This theorem allows us to assume that for a fluid particle with zero net forces will have constant circulation surrounding itself.

The results from above can be combined to derive the a model for the vorticity in order to describe behaviour of flow. For barotropic flow, we found that there exists an associated conserved value which is the circulation. Since Kelvin's theorem doesn't hold for baroclinic conditions, we can infer what the conserved quantity for the potential vorticity would be. We find that for some scalar  $\lambda$ ,

$$\Pi = \frac{\omega + 2\Omega}{\rho} \cdot \nabla \lambda \quad (17)$$

and thus, the scalar quantity is conserved if the material derivative of  $\Pi$  is equal to zero and the value  $\Pi$  is conserved if the equation Equation (17) is true.

### 2.3 Shallow-Water Model

The shallow-Water model is a relatively simple model with a set of dynamics that can be related to the activity of Jupiter's vortices. When considering this model, the "general equations" become restricted such that the atmosphere is in hydrostatic equilibrium and is also homogenous, such that  $\rho(r) = \rho$ . Additionally, we'll assume the large-scale model in order for the aspect depth ratio (comparing planet's radius with altitude range) to be minute. The system can be described by that shown in Figure 2.3.

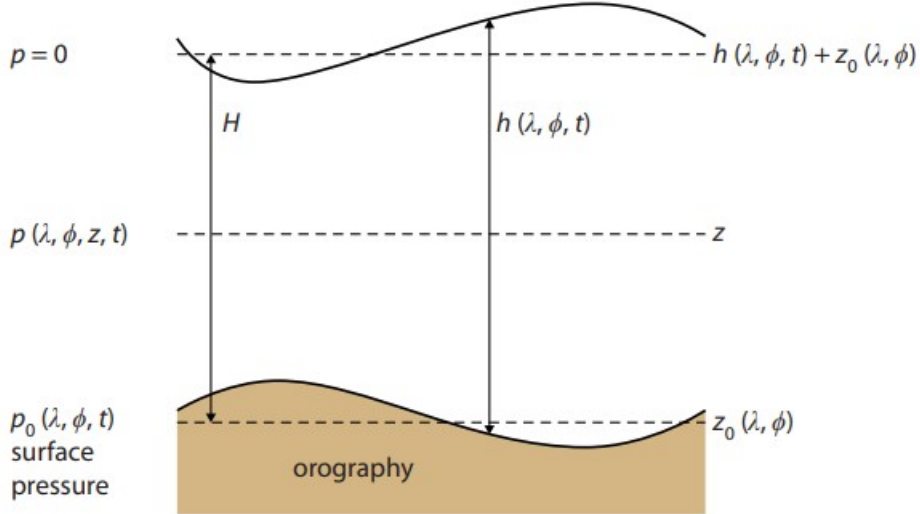


Figure 3: Illustration of the shallow-water Model: Above a non-uniform surface, characterized by the height  $z_0(\lambda, \phi)$ , an atmospheric region with vertical extent  $h(\lambda, \phi, t)$  exists. The metric  $\eta(\lambda, \phi, t)$  models the difference in altitude between the upper surface and the equilibrium point,  $H$ .

such that

$$\eta = z_0 + h - H \quad (18)$$

The following equations are combined to express the behaviour of shallow-water models.

$$\frac{\partial u}{\partial t} + (\vec{v} \cdot \nabla)u = -\frac{\partial(gh)}{\partial x} + fv + \Delta^m u + k(r)u_t \quad (19)$$

$$\frac{\partial v}{\partial t} + (\vec{v} \cdot \nabla)v = -\frac{\partial(gh)}{\partial y} + fu + \Delta^m v + k(r)v_t \quad (20)$$

$$\frac{\partial(gh)}{\partial t} = -gh\nabla \cdot \vec{v} + \Sigma S_{storm} + S_{mass} + S_{rad} \quad (21)$$

where:

- $gh$  is the height variable, or fluid thickness
- $v_t$  and  $u_t$  are the zonal and meridinal velocity terms
- $k(r)$  is the sponge strength

The storm shape is a suggestion of the mass pulse and is given by:

$$S_{\text{storm}} = s \times \exp\left[\frac{-R^2}{R_{\text{storm}}^2} - \frac{(t - t_0)^2}{\tau_{\text{storm}}^2}\right] \quad (22)$$

where:

- $R_{\text{storm}}$  is the radius of the storm
- $\tau_{\text{storm}}$  is the average lifetime of the storm
- $s$  is the maximum mass injection rate

To simplify the process of determining solutions to these equations, we can assume the applicability of the geostrophic adjustment. In doing so, we'll consider the general solution of the linearized shallow-water equations on an f-plane. We therefore can use the approximation of the bathtub vortex.

In this investigation, a 1-layer shallow water model is used. The shallow water model assumes shallow depth, which enables the hydrostatic approximation (the idea that the pressure at any point is due to the fluid above it). Additionally, the model assumes that the fluid is of constant density. It is evident that these approximations are not appropriate for Jupiter, since the 200km box that we are considering is not smaller than the height of the atmosphere. Additionally, Jupiter's atmosphere is composed of many gases of different densities.

## 2.4 Bathtub Vortex

The conditions for this linear model involve an isolated open surface liquid vortex, such that the vortex is generated by the force of gravity induced by the outflow of liquid material. This can be visualized by the replacement of the horizontal axis in Figure 2.3 with a flat line of constant value. To characterize this model, the Bernoulli function is obtained from the adjusted continuity equation, such that,

$$p = p_0 - \frac{1}{2}\rho_0 U^2(x) = gh + \frac{1}{2}(u^2 + v^2) \quad (23)$$

The vortex' behaviour can be characterized by the fluid discharge,  $q$ , which describes the asymptotic inflow. As a result of mass conservation, the value is expressed as,

$$q = \frac{Q}{2\pi h} = \frac{-2\pi r v_r h}{2\pi h} = \frac{\omega + f_o}{h} \quad (24)$$

- over the fluid particle displacement of the length of the vortex core,  $L = h$ .

As previously suggested, the potential vorticity of the system can be obtained due to conservation properties. Associated to this baroclinic flow, we can obtain the associated conserved quantity, given as the potential vorticity,

$$\Pi = \frac{\omega + 2\Omega}{\rho} \quad (25)$$

The transport velocities given in the previous equations can be determined using the expression for vorticity as a function of radial position,

$$\omega(r) = v_r(r, z) + \frac{z}{r} \frac{dv_r}{dr} h = \frac{1}{r} \frac{dv_r}{dr} h \quad (26)$$

The flux in vorticity can be determined through the evaluation of the the gradient of  $p$ . Components of  $\nabla p$  contribute to the corresponding flux components as,

$$f_u = qV - p_x f_v = -qU - p_y f_h = -U_x - V_y \quad (27)$$

The energy of the vortex can be found by integrating the energy of a fluid particle over some observation time, under the conservation of energy. Using the previous energy description, equation (1), one may find the energy for the vortex to be,

$$E = \frac{1}{2} \int_V dV \bar{\rho} (|\nabla_h \psi|^2 + \frac{b^2}{N^2}) \quad (28)$$

Evaluating the total energy for the condition of zero horizontal wind suggests the presence of another conserved quantity, one that suggests magnitude for the wave activity. This value is defined as the enstrophy,

$$Z = \int_S dS \frac{\pi^2}{2} = \frac{1}{2} \frac{1}{N} \int dz q^2 \quad (29)$$

## 2.5 Flow Instability

Flow instability refers to the tendency of a fluid flow to deviate from a smooth, laminar flow to an unsteady, turbulent flow.

### 2.5.1 Kelvin-Helmholtz Instability

The Kelvin-Helmholtz instability is a type of instability that occurs at the interface between two fluids of different velocities or densities. In this scenario, vortices are generated due to the shear between the two fluids, and these vortices can lead to flow instability. Mathematically, Kelvin-Helmholtz instability can be described using the linearized equations of fluid motion. The criterion for stability can be expressed in terms of the ratio of the density and velocity differences between the two fluids:

$$\mu = \frac{(\rho_2 - \rho_1)}{(v_2 - v_1)} \quad (30)$$

where  $\rho_1$  and  $\rho_2$  are the densities of the two fluids, and  $v_1$  and  $v_2$  are their velocities. If  $\mu$  is greater than a critical value, the interface between the two fluids will be unstable, and vortices and waves will be generated.

### 2.5.2 Rossby Number

The Rossby radius of deformation is the length scale at which effects from rotation are as important as those from gravity as buoyancy for the evolution of the flow of some disturbance. The modified version is given below.

$$L'_\beta = (\frac{1}{L_\beta^2} - \frac{1}{L_d^2})^{-\frac{1}{2}} \quad (31)$$

where:

- $L_\beta$  is the barotropic random turbulence
- $L_d$  is the deformation parameter

The equation of position for the Rossby waves can be taken as  $w$ , such that the expression defines the linear relationship between the local versions of the space-time frequency and the wave number as,

$$k = \frac{2\pi}{NL} \quad (32)$$

Combining the descriptions for the instability and wave concepts allows for the conceptualization of wave propagation as the Rossby-Wave Propagation. Applying this propagation method, it is easy to obtain the associated dispersion model for the waves due to large-scale assumptions that are made.

The surface and volume forces can then be used to determine expressions for the overall momentum. From the Navier-Stokes equations, we can apply the conservation of momentum, this requires that for the following stress tensor components,

$$\nabla \cdot \sigma_i = \frac{\partial \sigma_{ij}}{\partial x_j} \quad (33)$$

we have that,

$$\rho \frac{D\mathbf{v}}{dt} = \mathbf{f} - \nabla p + \nabla \cdot \sigma \quad (34)$$

Taking  $\mathbf{f} = \rho\mathbf{g}$ , and integrating both sides, we are left with the depth of the depression as

$$Lv_i \propto \lambda_i L_j \quad (35)$$

for  $i = 1, 2$  and  $j = x, y$

The relationship expressed in equation (33) can then be used to draw a conclusion regarding the solution for the equations of motion. For the bathtub vortex, as shown in (Lautrup, pp. 476), that integrating over  $\omega(r)$  allows for the determination of the depth as a function of radial position, as shown below.

$$\omega(r) = -W \exp -\frac{r^2}{a^2} \rightarrow rv_r(r)h_r(r) = - \int W \exp -\frac{r^2}{a^2} \rightarrow h(r) = -3 \exp -\frac{(r - \Delta r)^2}{Lv_i^2} \quad (36)$$

We'll apply basic vortex theory to a variety of "unsteady" scenarios in order to analyze the stability properties of various vortex systems. A particular example that we will examine involves the scenario of colliding vortices. This scenario involves the introduction of a vortex, of opposite sign, into a system with an active vortex, such that the two vortices are positioned orthogonally to one another. We may also review the case of vortex shredding, a phenomenon which occurs due to the effect of strong winds on vortices.

### 3 Specific Example: Jupiter

In this section, we will describe the specific problem that we are aiming to address. As mentioned, vortices are an essential component of the atmospheres of gaseous giant planets. Our plan is to specifically investigate Jupiter, mainly because of its prominent patterns and the wealth of data from space probes such as Juno.

One of the most famous vortices on Jupiter is the Great Red Spot, a massive storm that has been observed for centuries. In addition to the Great Red Spot, there are many other vortices on Jupiter, ranging in size from small, local disturbances to larger, longer-lasting storms. These vortices can take on a variety of shapes and forms, from oval-shaped storms to more irregular, turbulent patterns.



Figure 4: The Great Red Spot on Jupiter, a significant and persistent cyclonic storm. (Credit: NASA, Juno.)

The polar vortices on Jupiter are different from the more well-known Great Red Spot and other vortices on the planet. This is because the polar vortices are situated at the poles and are much colder than the rest of the planet's atmosphere. They also exhibit a different type of circulation, with winds flowing in a circular

pattern around the pole. In particular, the Juno mission found that the southern polar vortex is surrounded by a band of bright, swirling clouds that move in the opposite direction to the vortex itself.



Figure 5: Vortices near the polar region of Jupiter (Credit: NASA, Juno.)

These clouds are believed to be formed by the interaction between the vortex and the planet's magnetosphere, which causes charged particles to flow around the vortex and create visible disturbances in the atmosphere. In the north pole, there are eight vortices around a central vortex, and in the south pole there are five. The patterns and the individual vortices that define them have been stable since August 2016.

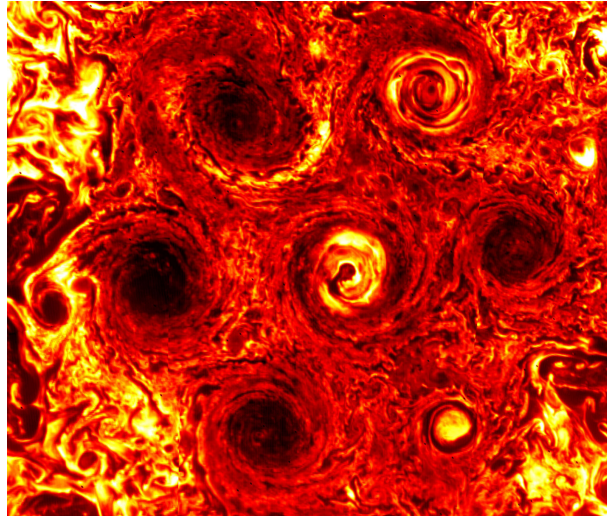


Figure 6: Hexagonal vortex pattern in the polar region of Jupiter (Credit: NASA, Juno.)

A particular pattern of interest on Jupiter is the hexagonal vortex pattern observed in the polar regions, shown in Figure 3. This pattern was first discovered by NASA's Voyager spacecraft in the late 1970s and has since been observed by subsequent missions, such as the Cassini spacecraft and the Hubble Space Telescope. The hexagonal vortex pattern on Jupiter consists of a persistent and stable arrangement of six roughly equally-sized, regularly spaced cyclonic (low-pressure) vortices arranged in a hexagonal shape around a single anticyclonic (high-pressure) vortex at the centre. This forms a hexagonal-shaped jet stream or "hexagon" that encircles Jupiter's pole. The hexagon is large, with each side measuring several thousand kilometres in length, and it extends vertically for several tens of kilometres in the planet's atmosphere. Possible

explanations for this pattern include Rossby waves and barotropic instability, but the true explanation is still up for debate.

## 4 Code

To numerically simulate the vortices, we will use a modified version of a 1-layer shallow water code developed by Dr. Francis Poulin. This code is two-dimensional, and its geometry is periodic in the  $x$  direction and channel-like in the  $y$  direction.

The numerical solution is based on the pseudo-spectral method, which is often used to solve differential and integral equations when there is a natural periodicity. The method involves representing the solution as a sum of complex exponentials, where the coefficients of the Fourier series are determined by projecting the solution onto a set of basis functions. These basis functions are chosen to be the Fourier modes, which are the complex exponentials of the form  $e^{ikx}$ , where  $k$  is an integer representing the wave number and  $x$  is the spatial coordinate. The term "pseudospectral" refers to the fact that the method combines the accuracy of spectral methods, which use global basis functions, with the flexibility of finite difference methods, which use local operators. In the pseudospectral Fourier method, the Fourier modes are used as global basis functions, but the differentiation and integration operations are performed using methods such as finite differences. The pseudospectral Fourier method has several advantages over other numerical methods. It can achieve high accuracy with relatively few grid points, and it can handle nonlinear and time-dependent problems. The Fourier method is used to calculate the velocities of the vortices in the frequency space.

The Adams-Bashforth method is a numerical technique for approximating the solution of ordinary differential equations (ODEs) using a fixed time step. Specifically, it is a predictor-corrector method that uses past values of the solution to estimate future values. The method works by using a polynomial approximation to the solution over a small time interval. The coefficients of this polynomial are determined by using past values of the solution and its derivatives. The polynomial is then used to approximate the value of the solution at the next time step. Some examples of parameters that need to be specified in the code include  $f_0$ , given by:

$$f_0 = 2\Omega \sin(\theta) \quad (37)$$

Where  $\theta$  can be found based on the period of the planet. For Jupiter, the day is 9 hours and 56 minutes long, or 0.414 of an Earth day. We also need to specify the depth  $H_0$  (thickness of the outer layer in which vortices occur) which must also be tuned for Jupiter, we estimate a depth of 500m. Additionally, the time step needs to be chosen as:

$$dt = \frac{0.2}{\sqrt{g \times h_0}} dx \quad (38)$$

in order to resolve the dynamics. The gravity of Jupiter is  $23.15 \frac{m}{s^2}$ . An initial run of the code is shown below,

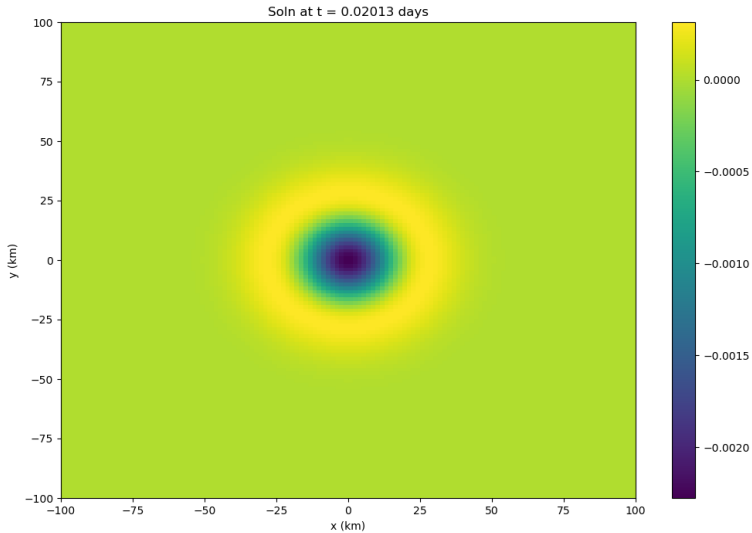


Figure 7: Initial run of the shallow water model code modified for Jupiter. This plot captures the spatial extent of the vortex, with the colour bar showing the vorticity in units of  $\frac{1}{s}$ . The runtime is for 0.2 of a Jupiter day (so about two hours), at a time-step of 3 seconds.

This is a stagnant, singular vortex. To add some interesting dynamics, we can introduce more vortices, along with spatial shifts in their initial locations. These shifts will be referred to as  $x_{shift}$  and  $y_{shift}$  for shifts in the x and y directions, respectively. In the following section, these more interesting vortex scenarios will be described. Overall, the main changes to the code to specify that it is Jupiter include the parameters  $g$ ,  $f_0$ , the orbital period, the constant depth, and the time-step. Clearly, these are not all the necessary parameters to specify vortex motion on Jupiter, but this investigation presents a simple case with the two-dimensional shallow water model.

## 5 Results

In this section, we will describe the results of the shallow-water code for three specific cases of vortex interactions. These cases involve the number of initialized vortices: where we investigate two (dipole), three (tripole), and six vortices. These cases were selected because they demonstrate some basic interactions between multiple vortices, allowing us to explore the dynamics of vortices with different polarities. Additionally, the case with six vortices was selected because of its particular significance in gas giants such as Jupiter.

### 5.1 Two Vortices (Dipole)

In the first case, we will initialize two vortices of opposite polarity, with one vortex being double the size of the other. The runtime is for 0.2 of a Jupiter day at a time-step of 3 seconds. The equation for the depth of these two vortices is given as:

$$h_B = -Ae^{(-\frac{(x-x_{shift})^2+(y-y_{shift})^2}{(LV_1)^2})} + Be^{(-\frac{(x+x_{shift})^2+(y-y_{shift})^2}{(LV_2)^2})} \quad (39)$$

Where in this case,  $A = 3$ ,  $B = 6$ ,  $x_{shift} = -10\text{km}$ ,  $y_{shift} = -20\text{km}$ ,  $LV_1 = 10\text{km}$ , and  $LV_2 = 20\text{km}$ . The vorticity plots for several instances in time are shown below.

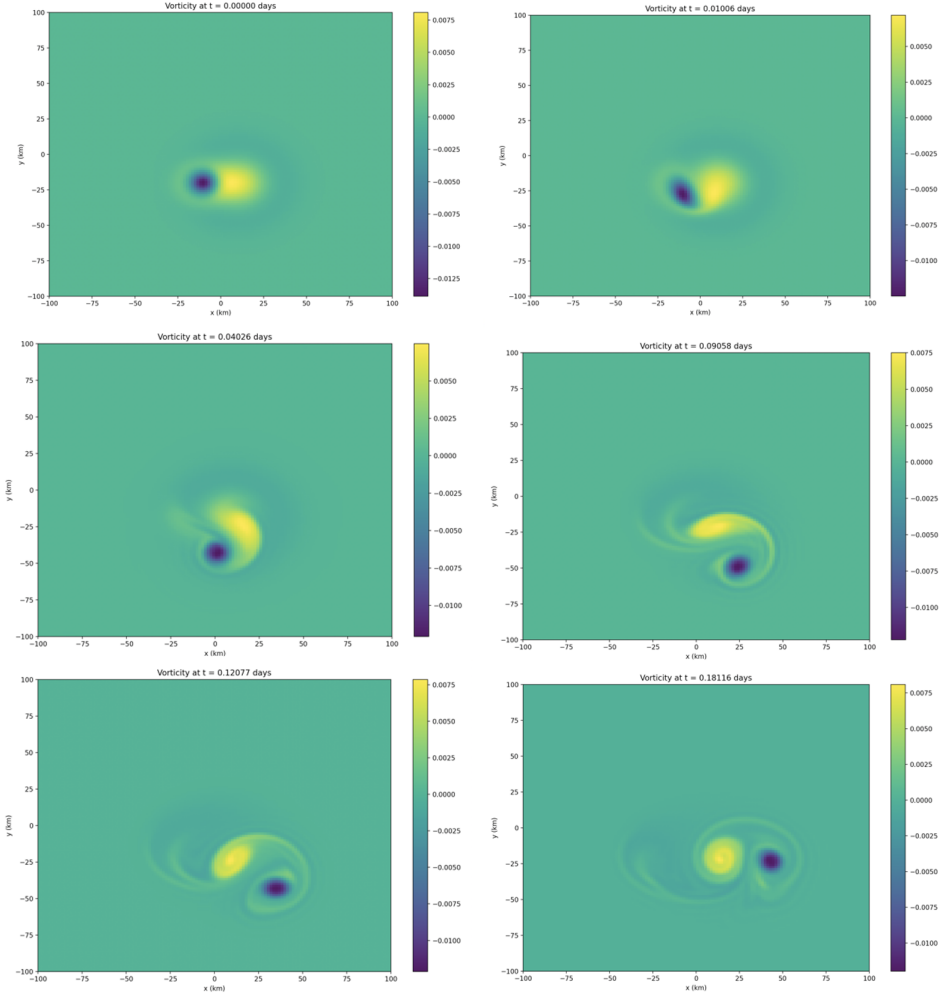


Figure 8: The vorticity (in  $\frac{1}{s}$ ) of two opposite polarity vortices shifted by  $x = 10$  km and  $x = -10$  km, respectively at  $y = 20$  km, with the negative vortex being double the strength of the other.

In the first frame, at  $t = 0s$ , we notice that the two vortices are next to one another, with the yellow spot being representative of the positive polarity vortex that is double the strength of the negative polarity vortex. As the interaction evolves in time, we notice that the dipole structure remains, and the opposite polarity of the vortices results in their spatial translation. The larger, more positive vortex moves up such that it can push down on the smaller, more negative vortex. This behaviour can be attributed to the Coriolis force (Equation (14)), which is a result of the rotation of Jupiter, causing moving objects to be deflected to the right in the northern hemisphere and to the left in the southern hemisphere.

Since the positive polarity vortex is twice as strong as the negative polarity vortex, it would experience a stronger Coriolis force. As a result, the positive vortex would tend to move towards the pole in the northern hemisphere, while the negative vortex would tend to move towards the pole in the southern hemisphere. By the Taylor-Proudman theorem, the slowly evolving flows do not vary along the direction of the rotation axis, and essentially behave like a two-dimensional flow. The flow is mainly azimuthal because of the rapid rotation, so that Coriolis accelerations balance those due to the radial pressure gradient. It's important to note that on Jupiter, the Coriolis force from the planet's rotation swirls air masses rising upwards. However, the cyclones on Earth rotate in the opposite direction from those on Jupiter. This is because on Jupiter, the vortices are formed when rising gas strives apart in the upper atmosphere. On Earth, however, they start at the bottom, where air converges and then rises. This behaviour for Jupiter is simulated in our code through

the shallow water approximation, where the fluid moves at the top and the bottom layer is assumed to have no movement.

As the vortices move and interact, they shed material in their wake, known as vortex shedding. This is why there is a tail-like structure apparent in the last time frame. Next, the velocity plots in the same time frames are shown below to visualize the direction in which the vortices move. The shape in the final time frame is similar to the vortex shapes that can be seen on Jupiter, which indicates that vortices with differing polarities are a significant reason for these patterns.

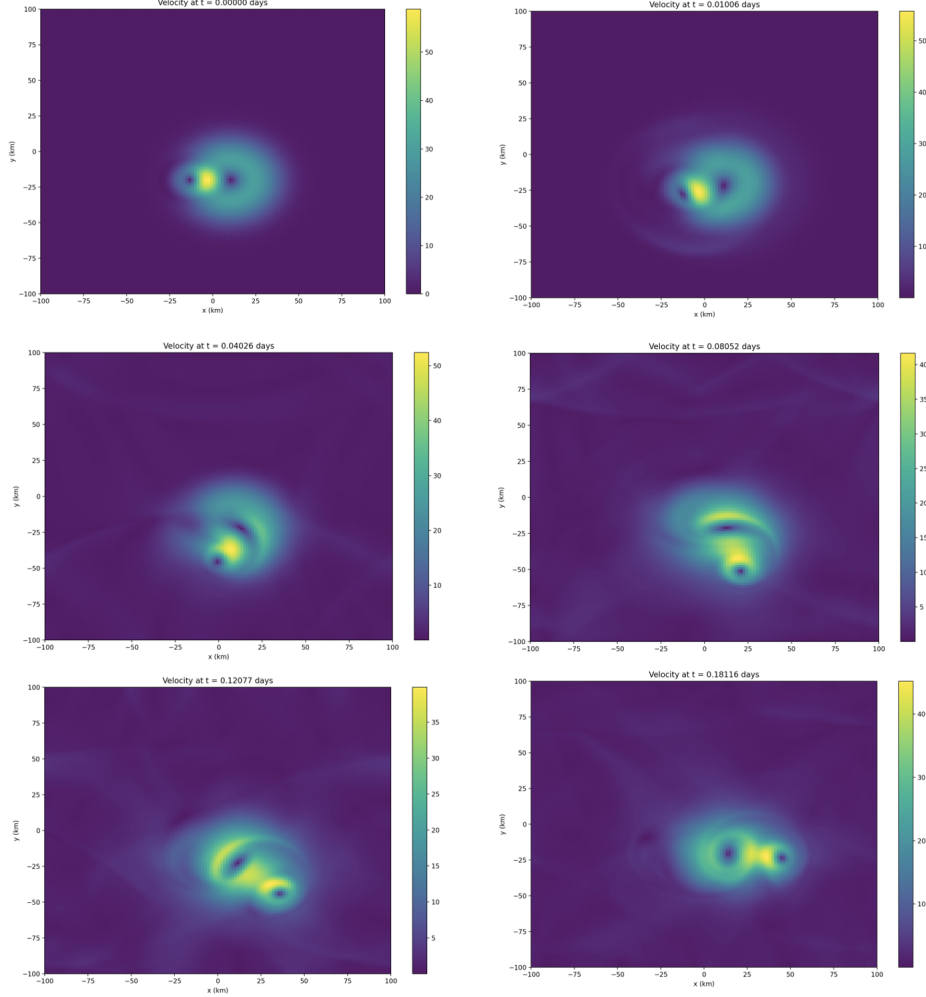


Figure 9: The velocity (in  $\frac{m}{s}$ ) of two vortices positioned at  $x = 10$  km and  $y = 20$  km, with one vortex being double the strength of the other.

From these plots, it can be deduced that the larger vortex has greater velocity in its outer regions, meaning that it initially has greater speed and thereby deflects the smaller vortex. As the system evolves, the greatest velocities are in between the centres of the two vortices. To illustrate the directionality of the velocity after this last time frame, we can do a quiver plot, which indicates the gradient of the velocity:

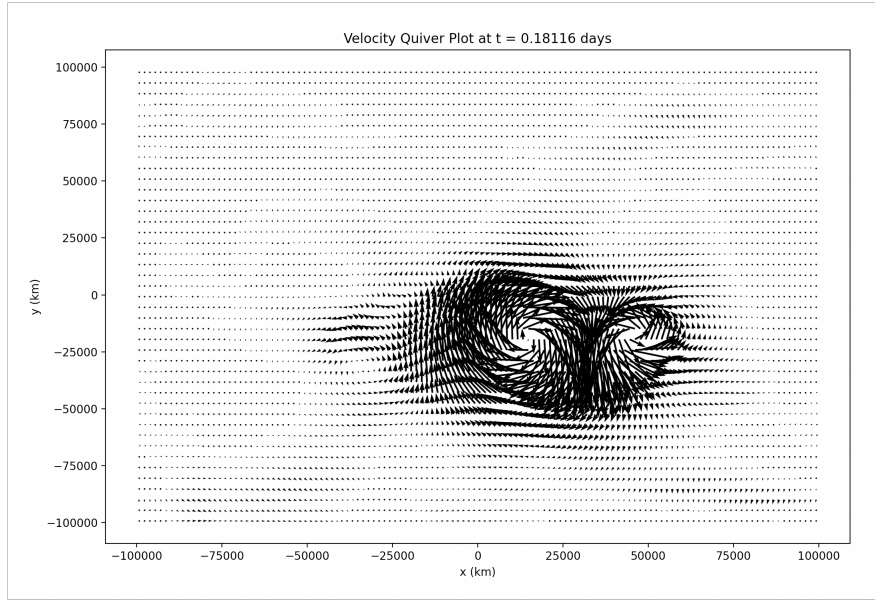


Figure 10: A quiver plot at  $t = 0.18116$  days displaying the direction of the velocity (in  $\frac{m}{s}$ ) of the two vortices positioned at  $x = 10$  km and  $y = 20$  km, with one vortex being double the strength of the other.

This quiver plot shows the gradient of the velocity at this instance in time, where we see larger arrows for larger velocities. The two dipoles have velocity gradients that point circularly inward, implying that the vortex will continue to translate as the Coriolis force affects the two dipoles.

Next, plots of the depth through time will be examined for this scenario of two dipoles. These plots will provide greater insight into the way in which the vortex depth varies. It's important to note that the shallow water model assumes a constant depth (500m in this case) for the fluid layer, but the depth of the vortex varies as stretching and squeezing occurs. For example, in a scenario where a vortex intensifies (and becomes more tightly wound), the vortex may stretch vertically, causing the vortex depth to decrease.

The plots are shown in Figure 11, but they will be discussed here. In the first frame, it can be noted that the smaller vortex has a positive depth, which indicates that the fluid height is higher than the reference depth level, representing an elevated region due to the presence of a vortex. This corresponds to the core of the vortex, where the fluid is lifted. As for the larger vortex, the depth is larger and negative, representing a depressed region due to the presence of a vortex. This means that the fluid is displaced downward. As the vortices interact in time, the depth of their cores become increasingly negative (up to about 50km), which makes sense since fluid is continuously being pulled down in the shallow water model due to gravity. Elliptical shapes of positive depth are apparent in the second frame, which evolve in time to produce more regions of positive depth. The ellipses of positive depth arise from the conservation of potential vorticity (PV) in the fluid. Potential vorticity is a quantity that is conserved in the absence of external forces in an inviscid, adiabatic fluid. When two vortices with opposite polarities interact, they can transfer potential vorticity from one vortex to the other. In the last four frames, there are some perturbations in the fluid in which there is positive depth, likely arising from the interaction between the two vortices.

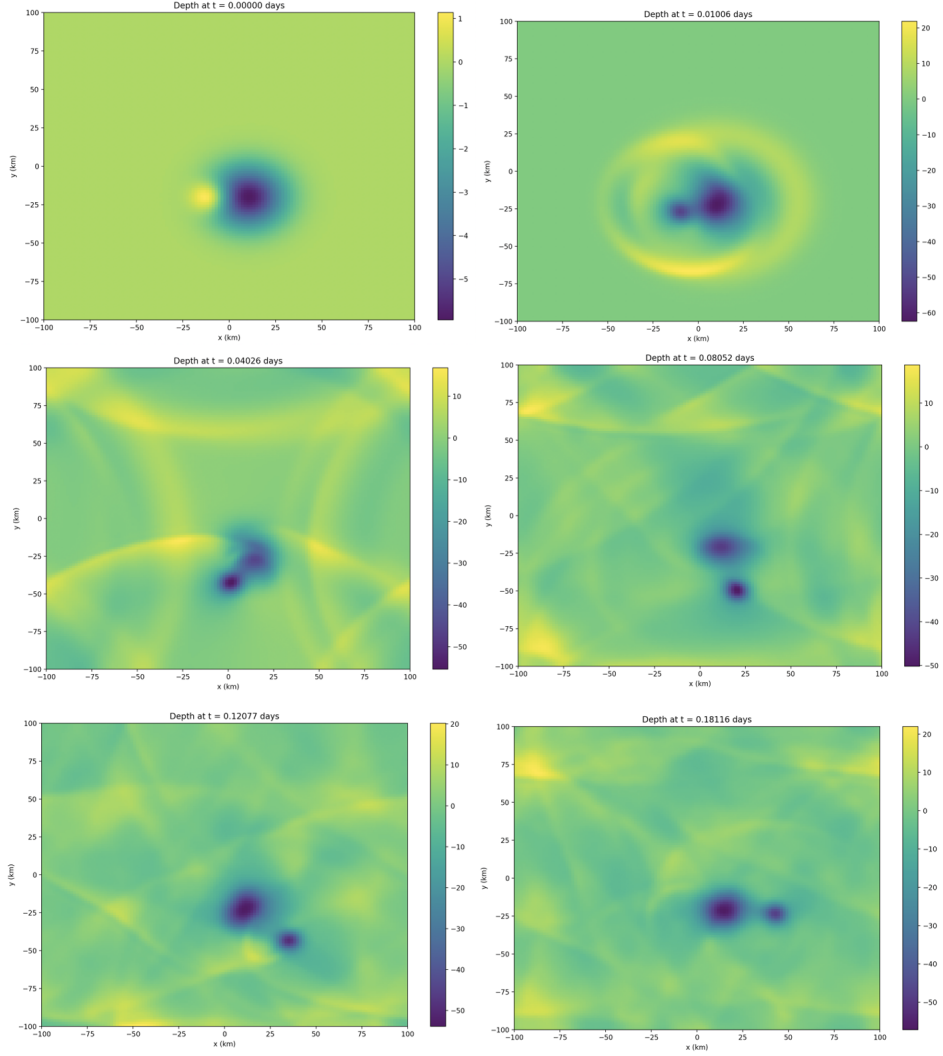


Figure 11: The depth (in  $m$ ) of two vortices positioned at  $x = 10 \text{ km}$  and  $y = 20 \text{ km}$ , with one vortex being double the strength of the other.

## 5.2 Three Vortices (Tripole)

In the next case, we will investigate the case of three initialized vortices, with negative, positive, negative polarities, respectively. The runtime for this simulation is again 0.2 of a Jupiter day, so about 2 hours. The equation governing the vortex depth is given as:

$$h_B = -Ae^{-\frac{(x-x_{shift})^2+(y-y_{shift})^2}{(LV_1)^2}} + Ae^{-\frac{(x)^2+(y-y_{shift})^2}{(LV_1)^2}} - Ae^{-\frac{(x+x_{shift})^2+(y-y_{shift})^2}{(LV_1)^2}} \quad (40)$$

where in this case,  $A = 3$ ,  $x_{shift} = 20 \text{ km}$ ,  $LV_1 = 10 \text{ km}$ . The plots for the vorticity over time are shown in Figure 12.

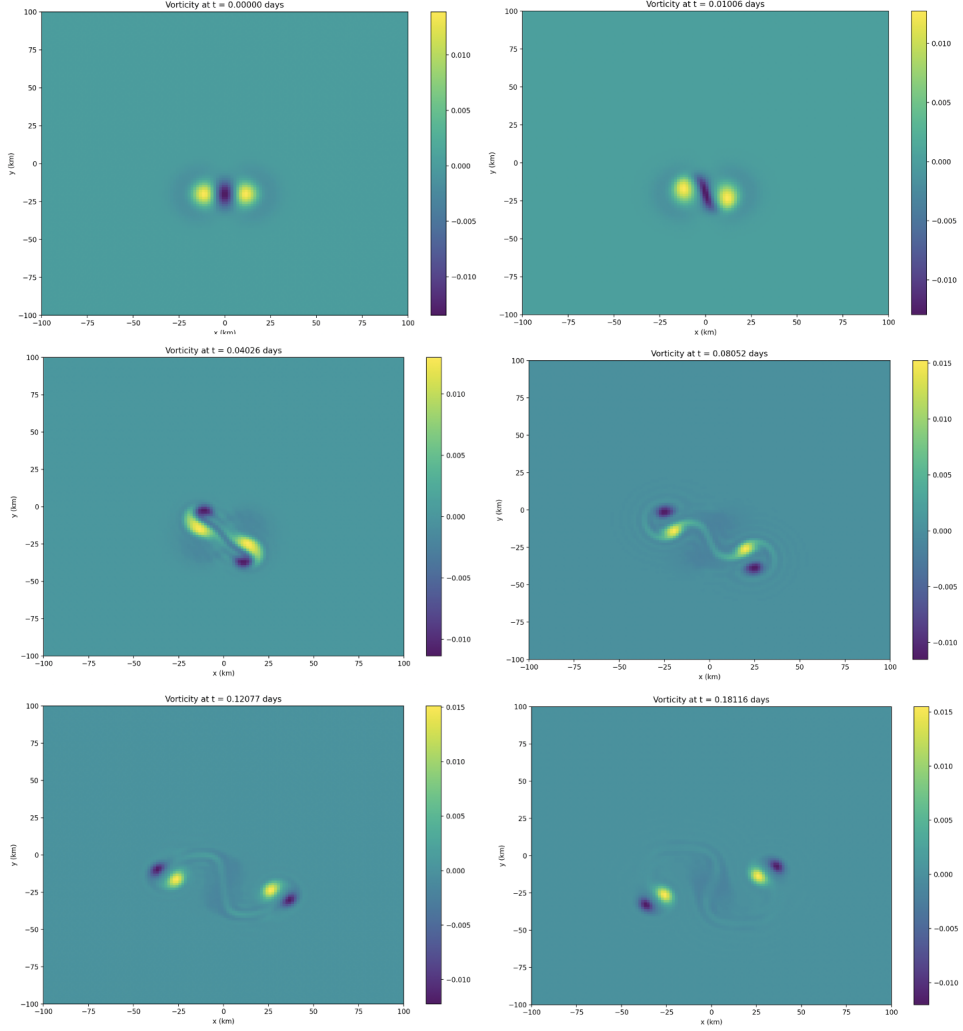


Figure 12: The vorticity (in  $\frac{1}{s}$ ) of three (with negative, positive, negative polarity, respectively) vortices. One vortex is shifted to the left by  $x = 20$  km, one vortex has no shift, and the last vortex is shifted to the right by  $x = 20$  km, all of them are shifted down by  $y = 20$  km.

In the first time frame, we see the three initialized vortices with the negative, positive, and negative polarities. The two negative vortices stretch the central positive vortex, two pairs of dipoles are created. The Coriolis force drives them in opposite  $y$  directions, and the interaction between the two pairs results in a shedding, which appears as a tail-like structure connecting the pairs. As done for the previous case, the plot of velocity is also shown below in Figure 13.

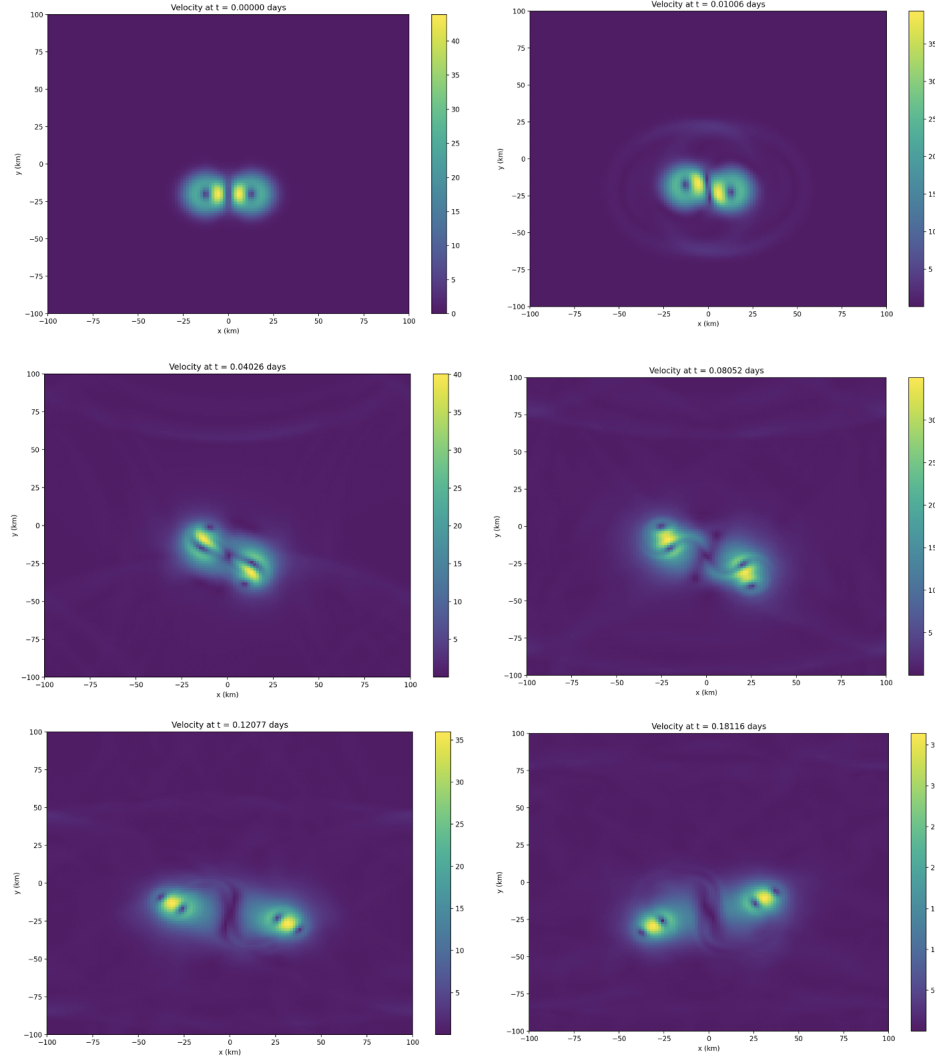


Figure 13: The velocity (in  $\frac{m}{s}$ ) of three (with negative, positive, negative polarity, respectively) vortices. One vortex is shifted to the left by  $x = 20$  km, one vortex has no shift, and the last vortex is shifted to the right by  $x = 20$  km, all of them are shifted down  $y = 20$  km.

In these plots, the time evolution of velocity can be investigated. In the first time frame, the two negative vortices have high velocities in their outer edges, with the highest velocities being at the edges that border with the central, positive vortex. This is because as the vortices approach each other, their swirling motions can cause the fluid between them to be "squeezed" or accelerated, leading to higher velocities at the points of interaction. This phenomenon arises due to the conservation of angular momentum, where the fluid between the vortices is forced to flow along a narrower path due to the constriction of the vortices, resulting in an increase in velocity. Through time, the dipoles form and the velocities remain high between the interaction of the poles in each pair, and the polarities of the pairs result in their respective spatial translations. To visualize the direction of the velocities, a quiver plot can be made for the last time frame, it is shown in Figure 14.

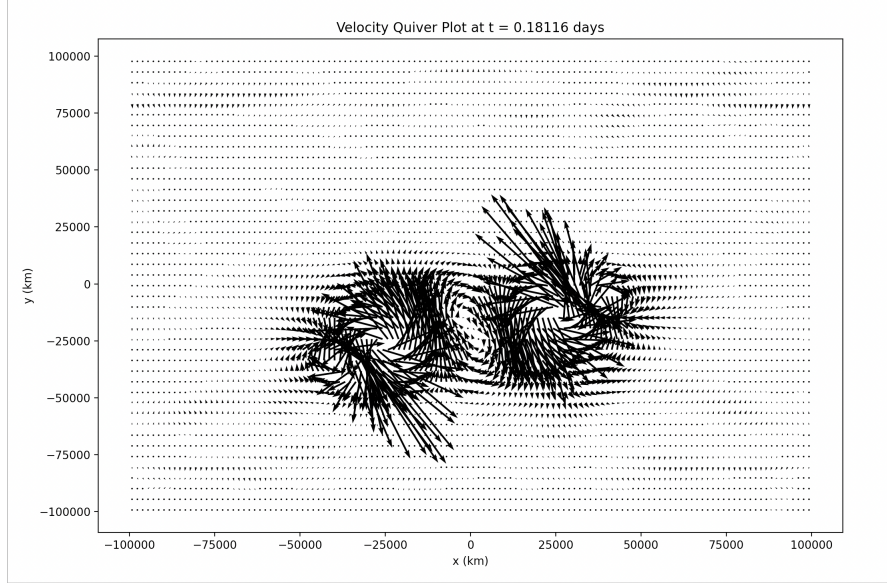


Figure 14: A quiver plot at  $t = 0.18116$  days displaying the direction of the velocity (in  $\frac{m}{s}$ ) of the three (with negative, positive, negative polarity, respectively) vortices. One vortex is shifted to the left by  $x = 20$  km, one vortex has no shift, and the last vortex is shifted to the right by  $x = 20$  km, all of them are shifted down by  $y = 20$  km.

From Figure 14, it is clear that the Coriolis effect drives the dipole pair on the left towards the bottom, and the dipole pair on the right towards the top. The Coriolis effect means that if the cyclonic vortex (negative polarity) of the dipole is stronger than the anticyclonic vortex (positive polarity), the dipole as a whole tends to move in the direction of the cyclonic vortex on Jupiter. It's important to note that the Coriolis effect depends on whether the vortices occur in the northern or southern hemisphere, but we have not specified it in this case. This means that the Coriolis force solely depends on Jupiter's period and the chosen  $f_0$  parameter.

Next, plots of the time evolution of the depth will be shown in Figure 15, but they will be discussed here. In these plots, it is clear that in the first time frame, the negative vortices are of greater negative depth (fluid driven below  $H_0$ ), whereas the positive vortex is of positive depth (accumulation of fluid above  $H_0$ ). Through time, there are elliptical regions of fluid accumulation above  $H_0$  (positive depth) at the outer edges of the vortices interacting, attributed to the conservation of potential vorticity between the three vortices, as described by Equation (17).

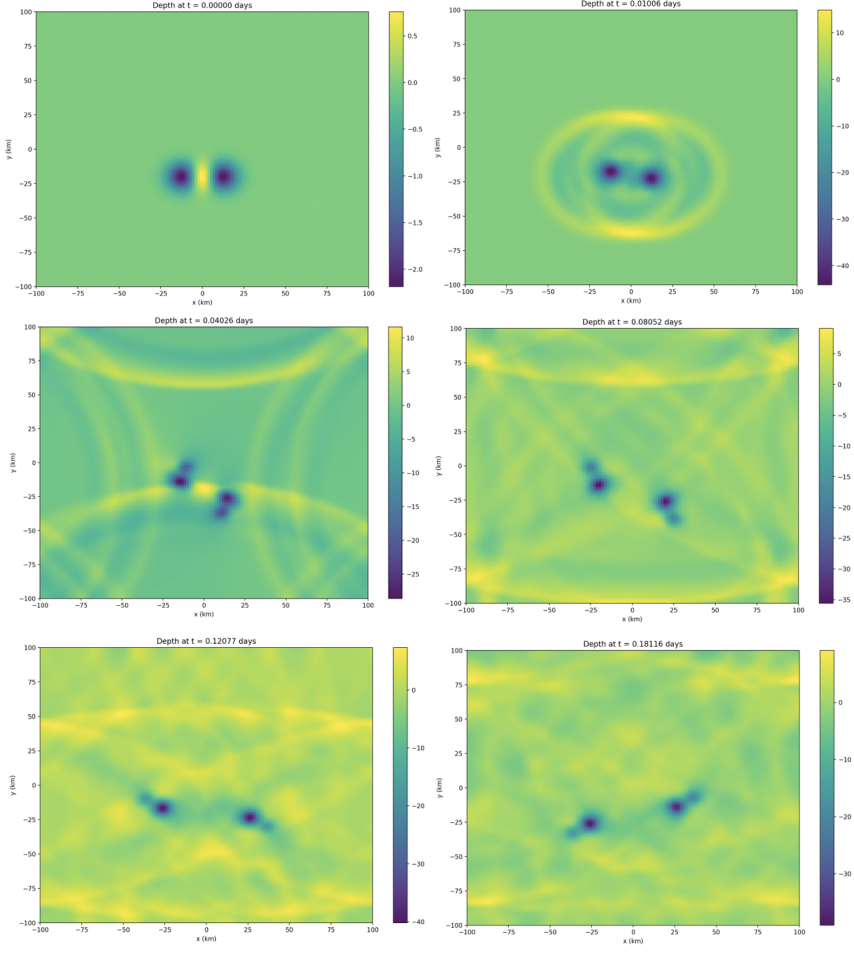


Figure 15: The depth (in  $m$ ) of three (with negative, positive, negative polarity, respectively) vortices. One vortex is shifted to the left by  $x = 20 \text{ km}$ , one vortex has no shift, and the last vortex is shifted to the right by  $x = 20 \text{ km}$ , all of them are shifted down by  $y = 20 \text{ km}$ .

### 5.3 Six Vortices (Hexagonal)

The final scenario is the initialization of six vortices with differing polarities, organized in the shape of a hexagon. As mentioned, this pattern is of particular significance to Jupiter. The runtime for this simulation is 0.4 of a Jupiter day, so about 4 hours. The equation describing the vortex depth is given in Equation (41).

$$h_B = Ae^{\left(-\frac{(x-x_{shift1})^2+(y+y_{shift})^2}{(LV_1)^2}\right)} - Ae^{\left(-\frac{(x-x_{shift2})^2+(y)^2}{(LV_1)^2}\right)} - Ae^{\left(-\frac{(x-x_{shift1})^2+(y-y_{shift})^2}{(LV_1)^2}\right)} - Ae^{\left(-\frac{(x+x_{shift1})^2+(y-y_{shift})^2}{(LV_1)^2}\right)} + Ae^{\left(-\frac{(x+x_{shift2})^2+(y)^2}{(LV_1)^2}\right)} + Ae^{\left(\frac{(x+x_{shift1})^2+(y-y_{shift})^2}{(LV_1)^2}\right)} \quad (41)$$

where  $A = 3$ ,  $x_{shift1} = 15 \text{ km}$ ,  $x_{shift2} = 30 \text{ km}$ ,  $y_{shift} = 30 \text{ km}$ , and  $LV_1 = 10 \text{ km}$ . The time evolution of the vorticity is shown in Figure 16.

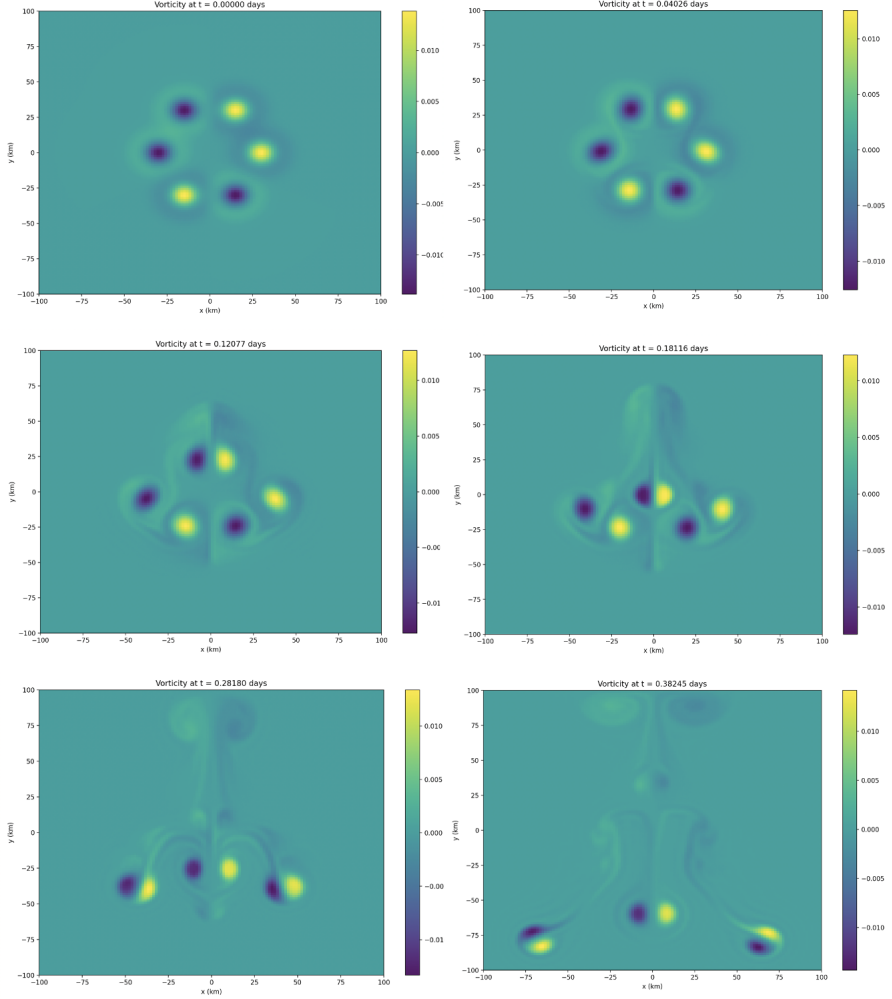


Figure 16: The vorticity (in  $\frac{1}{s}$ ) of six vortices of alternating polarity in hexagonal pattern. The top left vortex is shifted  $x = 15\text{km}$  to the left and  $x = 30\text{km}$  up, and the bottom right vortex is shifted  $x = 15\text{km}$  to the right and  $x = 30\text{km}$  down.

Initially, we see the vortices of differing polarities in a hexagonal pattern. Through time, pairs of dipoles are formed as vortices of opposite polarity move towards one another. Again, due to the Coriolis force, different dipole pairs move towards different directions. This results in several instances of vortex shedding (the tail-like structures). In the last time frame, it can be noted that the dipole pairs move towards the bottom of the bounded box. This large spatial movement is likely because of the various interactions between the dipoles, which are each of equal size and strength. Next, the plots for velocity through time are shown in Figure 17.

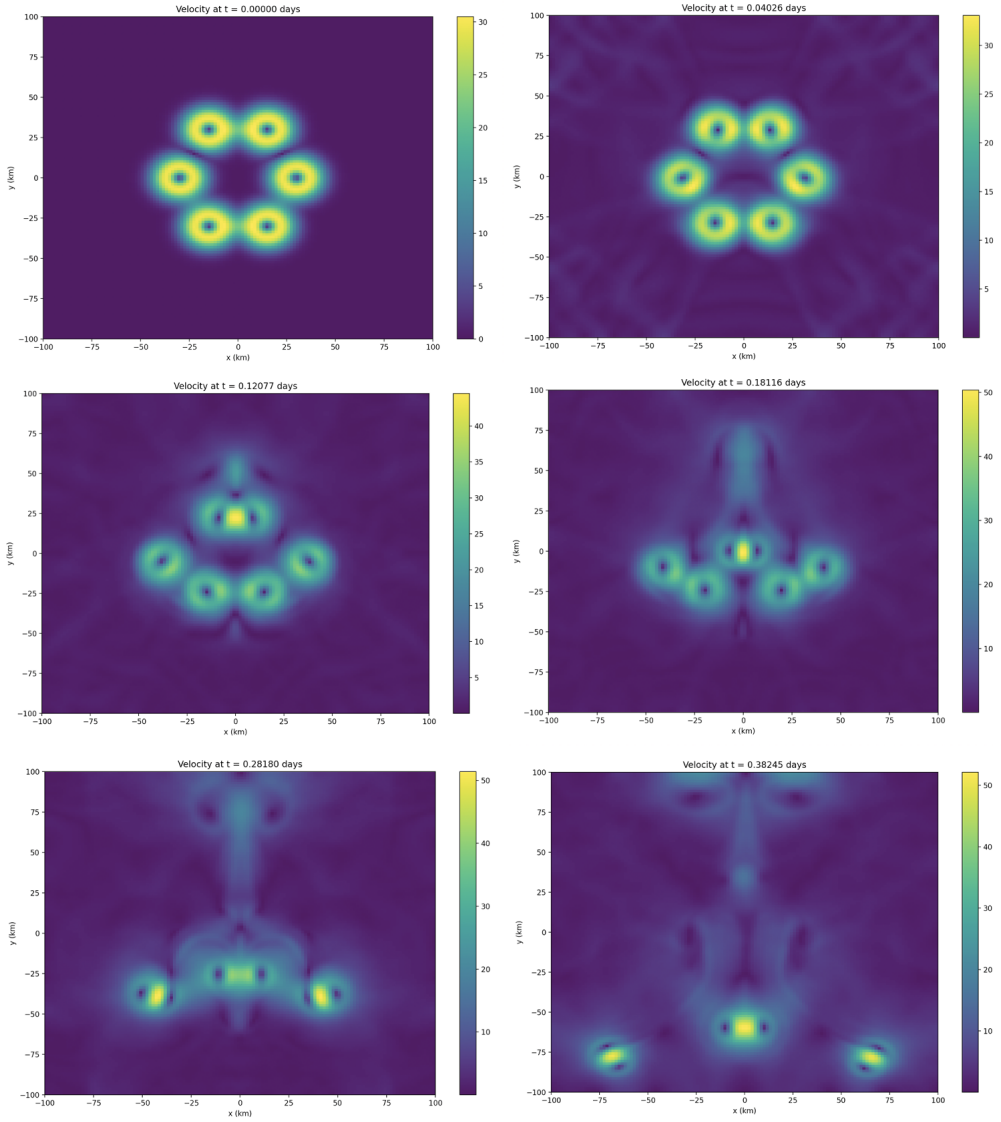


Figure 17: The velocity (in  $\frac{m}{s}$ ) of six vortices of alternating polarity in hexagonal pattern. The top left vortex is shifted  $x = 15\text{km}$  to the left and  $x = 30\text{km}$  up, and the bottom right vortex is shifted  $x = 15\text{km}$  to the right and  $x = 30\text{km}$  down.

In the first time frame, it is noted that the highest fluid velocities are at the outer edges of each vortex. As the dipoles begin to form, we see the highest velocities at the interaction between the two poles. The highest velocities increase from  $30 \frac{m}{s}$  (in the first time frame) to about  $50 \frac{m}{s}$ . To visualize the directionality of the dipole pairs in the last time frame, we can again make a quiver plot, shown in Figure 18.

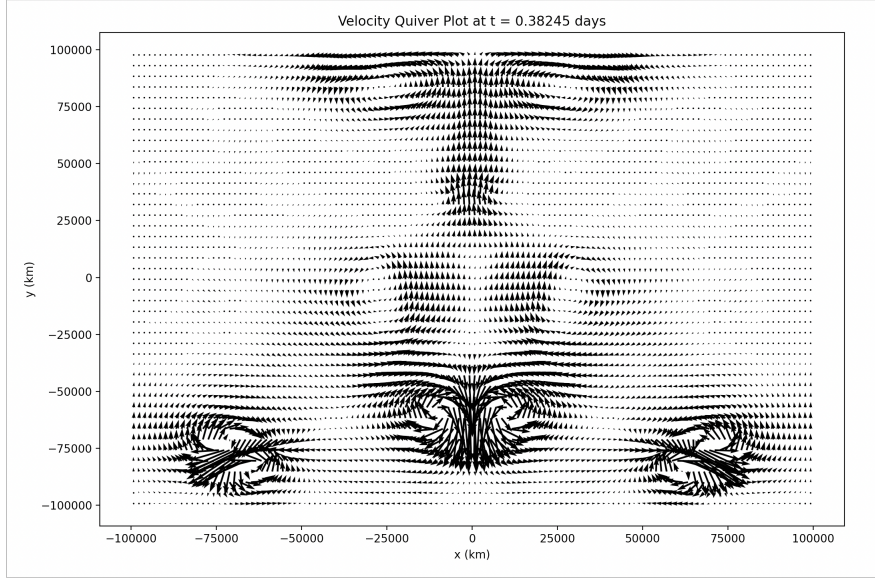


Figure 18: A quiver plot at  $t = 0.38245$  days displaying the direction of the velocity (in  $\frac{m}{s}$ ) of six vortices of alternating polarity in hexagonal pattern. The top left vortex is shifted  $x = 15km$  to the left and  $x = 30km$  up, and the bottom right vortex is shifted  $x = 15km$  to the right and  $x = 30km$  down.

From this plot, it is clear that the dipole pairs will continue to move down. This simulation includes periodic boundary conditions, which are not representative of the actual boundaries on Jupiter, meaning that continuing this simulation would not be accurate spatially. Next, the plots of the depth are shown in Figure 19, they will be discussed here.

In the first time frame, we see regions (ellipses) of positive depth forming around the vortex cores, this is due to the conservation of potential vorticity, where there is an ellipse forming for each vortex. As the vortices start interacting, these regions of positive depth grow spatially, resulting in a web-like structure throughout the box. It is likely that for a larger runtime, more vortices could arise from the interaction of these positive depths (however, we decided to stop the simulation before the periodic boundary conditions kicked in). The vortices themselves all have negative depth, and as they interact to become dipoles, they maintain this negative depth. The fluid composing the vortex cores sinks to about 40km.

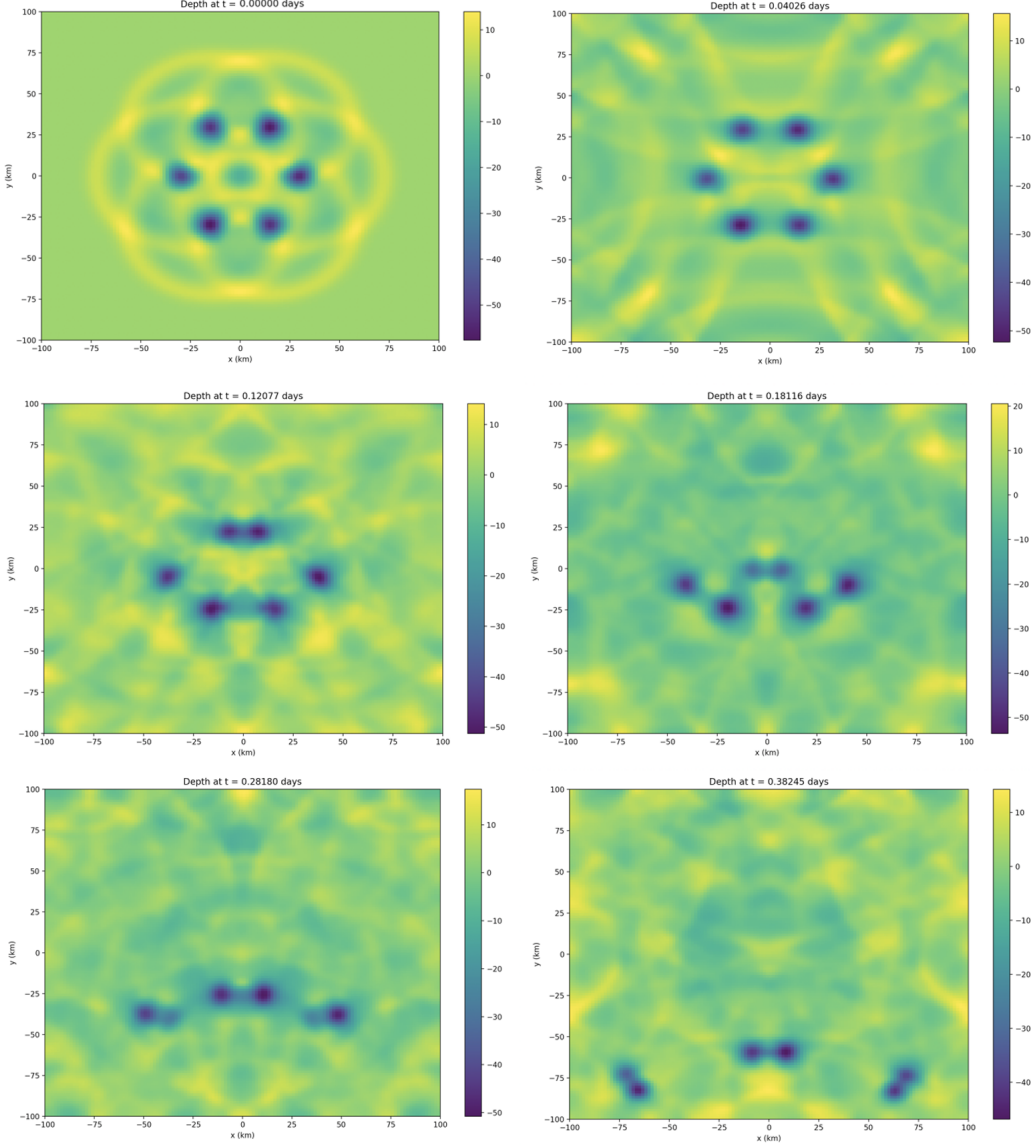


Figure 19: The depth (in  $m$ ) of six vortices of alternating polarity in hexagonal pattern. The top left vortex is shifted  $x = 15\text{km}$  to the left and  $x = 30\text{km}$  up, and the bottom right vortex is shifted  $x = 15\text{km}$  to the right and  $x = 30\text{km}$  down.

Overall, these simulations demonstrated:

- **Interaction and merging:** Vortices of opposite polarities, such as cyclonic and anticyclonic vortices, can interact and merge with one another. The relative strengths, sizes, and initial positions of the vortices can influence the outcome of these interactions. Merging of vortices can result in changes in their shapes, strengths, and movements, leading to the formation of larger or more stable vortices.
- **Vortex dynamics:** The complex dynamics of vortices, including their rotational motion, stretching, tilting, and twisting. Vortices can exhibit intricate and sometimes chaotic behavior, depending on the parameters of the simulation. The Coriolis force, which arises from the rotation of the planet or fluid, plays a crucial role in determining the dynamics of vortices, including their rotational direction and translation.

- **Vortex shedding:** Simulations have shown that vortices, especially in the context of vortex dipoles and tripoles, can shed smaller vortices periodically. These shed vortices can form organized structures in the wake of the larger vortices, such as vortex filaments and tubes, as described in the previous answer. Vortex shedding can lead to the formation of complex patterns and can affect the overall evolution and movement of the vortices.
- **Stability and longevity:** The stability and longevity of vortices can depend on their initial conditions, their relative positions, and the background flow. Vortices can exhibit different behaviors, ranging from short-lived and transient vortices to long-lived and stable vortices. The dynamics of vortices can also be influenced by the presence of other vortices or perturbations in the flow. In these simulations, the vortices moved on scales of hundreds of kilometres in a few hours, which may be faster than the actual spatial movement of vortices on Jupiter. The Great Red Spot, for example, is stable and has been for hundreds of years. This means that the vortices that compose it are so stable that they persistently form a high pressure region. For our simulation of the hexagonal formation, we saw that the vortices formed dipole pairs which spatially moved hundreds of kilometres in the span of 4 hours, which is not the case for the polar vortices which display these hexagonal structures on Jupiter.

## 6 Conclusion

In conclusion, the simulation of vortices on gas giants such as Jupiter using the two-dimensional shallow water model proved to be an effective tool for understanding the complex dynamics of these planets. By approximating the solutions of the partial differential equations governing these vortices in terms of a Fourier series (in the pseudospectral method), the method enables us to accurately capture the behavior of these large-scale atmospheric features.

Although the shallow water model makes assumptions that are not representative of Jupiter, such as constant density, the assumption of a shallow atmosphere, and two-dimensional behaviour, it was effective at demonstrating the interaction of multiple vortices and how they may give rise to the complicated shapes seen on Jupiter. The Jovian atmosphere is incredibly complicated, and a refined model that takes all the required variables into account is nearly impossible, so these approximations make reasonable sense (particularly so given the constraints of this report). The three simulations presented in this report showed the ways in which dipoles and tripoles form and interact, and how they give rise to more involved structures. The case with the initial hexagonal formation was of particular interest as it is a formation that is frequently seen on Jupiter, although we saw that the dipoles moved away very quickly spatially. These rapid movements are definitely attributed to the selected initial conditions, and the way in which we modelled the vorticity depth and their relative sizes. More investigation into the initial conditions required to simulate the time scales of Jupiter vortices would be a recommended way to extend this analysis. Some other analysis techniques involve studying the pressure and tangential velocities through time, or using a model more complex than the shallow water model to simulate the three-dimensional behaviour.

Overall, these simulations have revealed the intricate interactions, shedding behaviors, stability, and pattern formation of vortices, shedding light on their behaviors in natural phenomena such as atmospheric vortices on planets like Jupiter.

## References

- [1] Achatz, U. (2022). The Dynamics of the Shallow-Water Equations. In: Atmospheric Dynamics. Springer Spektrum, Berlin, Heidelberg. [https://doi.org/10.1007/978-3-662-63941-2\\_5](https://doi.org/10.1007/978-3-662-63941-2_5)
- [2] Lautrup, B. (2019). Physics of continuous matter: Exotic and everyday phenomena in the macroscopic world. CRC Press.
- [3] Li, C., Ingersoll, A. P., Klipfel, A. P., & Brettle, H. (2020). Modeling the stability of polygonal patterns of vortices at the poles of Jupiter as revealed by the Juno Spacecraft. *Proceedings of the National Academy of Sciences*, 117(39), 24082–24087. <https://doi.org/10.1073/pnas.2008440117>
- [4] Marcus, P. S. (1993). Jupiter's Great Red Spot and other vortices. *Annual Review of Astronomy and Astrophysics*, 31(1), 523–569. <https://doi.org/10.1146/annurev.aa.31.090193.002515>
- [5] Brueshaber S.R. (2020). Accumulation of Polar Vorticity on Giant Planets: Towards a Three-Dimensional Theory. Western Michigan University: Dissertations. <https://scholarworks.wmich.edu/dissertations/3655/>
- [6] Brueshaber, S. R., Sayanagi, K. M., &; Dowling, T. E. (2019). Dynamical regimes of giant planet Polar Vortices. *Icarus*, 323, 46–61. <https://doi.org/10.1016/j.icarus.2019.02.001>
- [7] Beffa, C. 2D-shallow water equations basics - applications - fluvial. (n.d.). Retrieved April 13, 2023, from [https://www.fluvial.ch/m/Hydraulics2\\_ShallowWater\\_2008.pdf](https://www.fluvial.ch/m/Hydraulics2_ShallowWater_2008.pdf)
- [8] Beffa, C. 2D-shallow water equations basics - applications - fluvial. (n.d.). Retrieved April 13, 2023, from [https://www.fluvial.ch/m/Hydraulics2\\_ShallowWater\\_2008.pdf](https://www.fluvial.ch/m/Hydraulics2_ShallowWater_2008.pdf)
- [9] Cai, Tao Chan, Kwing Mayr, Hans. (2021). Deep, Closely-Packed, Long-Lived Cyclones on Jupiter's Poles.
- [10] Mitchell, D. M., Scott, R. K., Seviour, W. J. M., Thomson, S. I., Waugh, D. W., Teanby, N. A., Ball, E. R. (2021). Polar vortices in planetary atmospheres. *Reviews of Geophysics*, 59, e2020RG000723. <https://doi.org/10.1029/2020RG000723>
- [11] University of Exeter. (n.d.). Retrieved April 13, 2023, from <https://empslocal.ex.ac.uk/people/staff/gv219/ecmm719/ess-ecmm719.pdf>
- [12] Wikimedia Foundation. (2023, March 30). Great Red Spot. Wikipedia. Retrieved April 12, 2023, from [https://en.wikipedia.org/wiki/Great\\_Red\\_Spot](https://en.wikipedia.org/wiki/Great_Red_Spot)
- [13] Greicius, T. (2015, March 13). Juno Image Gallery. NASA. Retrieved April 12, 2023, from [https://www.nasa.gov/mission\\_pages/juno/images/index.html](https://www.nasa.gov/mission_pages/juno/images/index.html)
- [14] Scarica, P., Grassi, D., Mura, A., Adriani, A., Ingersoll, A., Li, C., et al. (2022). Stability of the Jupiter southern polar vortices inspected through vorticity using Juno/JIRAM data. *Journal of Geophysical Research: Planets*, 127, e2021JE007159. <https://doi.org/10.1029/2021JE007159>
- [15] NASA. (2022, October 17). Jupiter: In depth. NASA. Retrieved April 12, 2023, from <https://solarsystem.nasa.gov/planets/jupiter/in-depth/>
- [16] Adams methods. (n.d.). Retrieved April 12, 2023, from [https://web.mit.edu/10.001/Web/Course\\_Notes/Differential\\_Equations\\_Notes/node6.html](https://web.mit.edu/10.001/Web/Course_Notes/Differential_Equations_Notes/node6.html)
- [17] Pseudospectral methods - welcome to the geophysics homepage. (n.d.). Retrieved April 13, 2023, from [https://www.geophysik.uni-muenchen.de/\\_igel/Lectures/NMG/04\\_pseudospectralmethods.pdf](https://www.geophysik.uni-muenchen.de/_igel/Lectures/NMG/04_pseudospectralmethods.pdf)